analytical chemistry

pubs.acs.org/ac Article

Concentric DNA Amplifier That Streamlines In-Solution Biorecognition and On-Particle Biocatalysis

Peng Yang, Yongya Li, Sean D. Mason, Fangfang Chen, Junbo Chen,* Rongxing Zhou, Juewen Liu, Xiandeng Hou, and Feng Li*

Cite This: *Anal. Chem.* 2020, 92, 3220−3227 Read Online

ACCESS | Metrics & More | Article Recommendations | Supporting Information

ABSTRACT: Colloidal nanoparticle biosensors capable of on-particle biocatalysis are powerful tools for amplified detection of biomolecules. The development and practical uses of such concentric amplifiers can be complicated because of the on-particle biorecognition that involves varying interfacial factors at the biomolecule−nanoparticle interfaces. Herein, we reason that a nanoparticle biosensor equipped with an in-solution biorecognition element may be better fabricated, predicted, controlled, and performed. The in-solution biorecognition shall also be streamlined with the on-particle biocatalysis so that the overall analytical and kinetic performance is not compromised. As a testbed, we introduce a concentric DNA amplifier driven by an enzyme-powered three-dimensional DNA nanomachine, where a DNA walker can be instantly assembled onto a spherical nucleic acid (SNA) track through a polyadenosine anchor. As such, the free DNA walker can participate in reactions in a homogeneous solution before assembling to the SNA track. The instant and stable assembly enabled by both adsorption and complementary base pairing also ensures rapid on-particle biocatalysis. We demonstrate that the in-solution biorecognition effectively eliminates the binding hindrance encountered by the on-particle biorecognition and thus significantly reduced energy barriers for the detection of nucleic acids and proteins. Because of the in-solution biorecognition, our system can also be plugged readily into complex DNA strand displacement networks for rapid signal amplification.

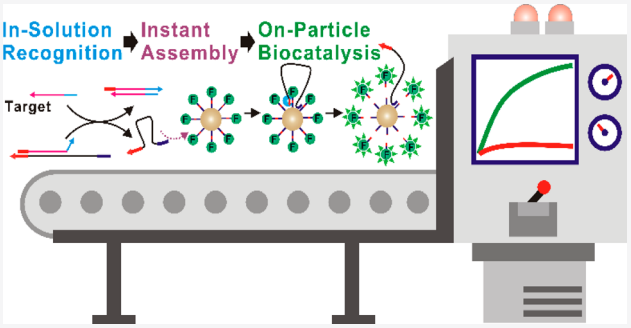

Colloidal nanoparticle biosensors have been of great interest for biological and biomedical applications.[1−4] Because of their unique size and material dependent optical, electrical, and magnetic properties, nanoparticles are often adopted as high-performance labels to improve the sensitivity for biomolecular detection and imaging.[5,6] When densely functionalized with substrates, the nanoparticle−substrate conjugates were also found to accelerate enzymatic reactions through intraparticle interactions.[4,7−11] Building upon the unique on-particle biocatalysis, several "concentric" amplifiers have been recently created featuring rapid signal transduction and amplification.[7−17] For example, Algar et al. observed that polyvalent peptide−quantum dot conjugates enhanced proteolytic acitivities through localized interfacial "hopping" interactions.[7,8] We and several other research groups have developed a series of three-dimensional DNA nanomachines (3DDN) with accelerated enzymatic cleavage through intraparticle DNA walking along spherical nucleic acid (SNA) tracks.[11−17]

To take full advantages of on-particle biocatalysis for biosensor development, the design of an efficient biorecognition element is equally important. However, biorecognition at the biomolecule−nanoparticle (bionano) interface depends strongly on varying interfacial factors, such as adsorption, multivalence, orientation, cooperativity, and binding hindrance.[9−11] For a simple DNA hybridization reaction at a DNA−AuNP interface, the ratio between surface and bulk equilibrium constants were observed to range from 10^{-16} to 10^{13}, spanning 29 orders of magnitude.[18−21] The kinetics of DNA hybridiztion on DNA−AuNP was also reported to be hindered by the nonspecific adsorption and nearest neighbor effects.[22] The influence of such interfacial factors to the binding between proteins and nanoparticles (e.g., the formation of protein corona) was found to be even more profound.[9,10,23]

For biosensor development, the complexity of the on-particle biorecognition at the bionano interface leads to two main challenges. First, molecular interactions are complicated by multiple interfacial factors and thus become much less predictable compared to the in-solution biorecognition. Extensive experimental or in silico optimization/modification

Received: October 31, 2019
Accepted: January 20, 2020
Published: January 20, 2020

https://dx.doi.org/10.1021/acs.analchem.9b04964
Anal. Chem. 2020, 92, 3220−3227

may be required to achieve the optimal target binding.[18−24] Second, many interfacial factors, such as adsorption, orientation, and steric hindrance, often result in unfavorable thermodynamic and kinetic barriers that significantly weaken the overall analytical performance of biosensors.[9−11,13,25] In such cases, we reason that a nanoparticle biosensor equipped with an in-solution biorecognition element may be better fabricated, predicted, controlled, and performed. The in-solution biorecognition shall also be streamlined with the on-particle biocatalysis so that the overall analytical and kinetic performance is not compromised. Herein, we introduce a concentric DNA amplifier that streamlines in-solution biorecognition and on-particle biocatalysis via an instant DNA assembly on a DNA−AuNP interface (Scheme 1). We

Scheme 1. (A) Schematic illustration of in-solution biorecognition vs. on-particle biorecognition. When the ligands (L) are densely functionalized on a single nanoparticle, possible binding hindrances may arise for the binding between the ligands and the receptor (R) because of one or multiple interfacial factors, including orientation, steric hindrance, and charge repulsion. On the other hand, the enzymatic reactions can be accelerated by the on-particle biocatalysis (B) because of the intraparticle interactions and drastically increased local substrate (S) concentrations. We aim to integrate the advantages of in-solution biorecognition with those of on-particle biocatalysis via an instant, one-step DNA assembly strategy.

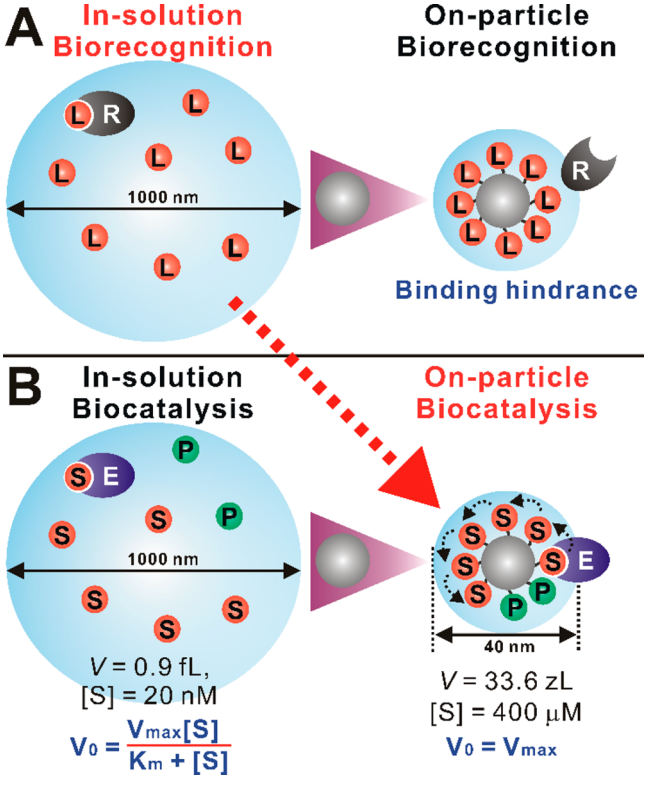

demonstrated that the combination of in-solution biorecognition and on-particle biocatalysis effectively reduced thermodynamic barriers of nanoparticle biosensors and thus improved the analytical performance for the detection of nucleic acids and proteins. As the biorecognition element is decoupled from the on-particle signal amplification, this concentric DNA amplifier can also be plugged readily into complex DNA networks for applications to biosensing and DNA computing.

EXPERIMENTAL SECTION

Materials. DNA sequences (listed in Table S1) were synthesized and modified by Integrated DNA Technologies (Coralville, IA, United States). All sequences were purified by HPLC and quantified using absorbance at 260 nm. Solutions of gold nanoparticles (AuNPs, 20 nm in diameter), TWEEN20, dithiothreitol (DTT), sodium chloride (NaCl), sodium iodide (NaI), magnesium chloride hexahydrate ($MgCl_2 \cdot 6H_2O$), streptavidin, 10× phosphate buffered saline (PBS, pH = 7.4), and 100× Tris-EDTA buffer (TE, pH = 7.4) were purchased from Sigma (Oakville, ON, Canada). Nicking endonuclease (Nb.BvCI), 10× CutSmart Buffer, and dATP solution were purchased from New England Biolabs Ltd. (Whitby, ON, Canada). Polyclonal antibiotin antibody was purchased from Abcam (Mississauga, ON, Canada). All solutions were prepared using NANOpure water (>18.0 MΩ) produced from an Ultrapure Milli-Q water system.

Preparation of SNA Tracks for 3DDNv1.0 and 3DDNv2.0. The SNA track for 3DDNv1.0 was prepared using a protocol modified from a previous report by our lab.[1] Briefly, the thiolated DNA walker and substrate oligonucleotides were mixed at a ratio of 1 to 20. A 20 μL solution of this mixture containing 0.25 μM walker and 5 μM substrates was mixed with 500 μL of a 1 nM concentration of AuNPs. This mixture was incubated at room temperature for 12 h and then was slowly mixed with 20 μL of 3 M NaCl, followed by 10 s of sonication. This process of salt aging was repeated three times with 1 h intervals. After incubation, the solution was centrifuged at 13 500 rpm for 30 min to separate the SNA track from the unreacted reagents. The tracks were washed three times with 1× PBS buffer containing 0.1% TWEEN20 and finally redispersed in PBS buffer.

For preparing the SNA track for 3DDNv2.0, a 20 μL solution containing a 5 μM concentration of substrates was mixed with 500 μL of 1 nM AuNPs for a low-density SNA track. A 20 μL solution containing 50 μM substrates was mixed with 500 μL of 1 nM AuNPs for a high-density SNA track. The salt aging and washing protocols were the same as mentioned above. To assemble the DNA walker, a walker oligonucleotide (typically 1 nM) with a polyA anchor was mixed with the SNA track (typically 100 pM). A fully functional 3DDNv2.0 is achieved immediately after mixing the two components.

Characterization of SNA Tracks. After preparation, UV−vis spectrosocopy was used to characterize the quality of the SNA track as well as determine the concentration of the track using the protocol we established previously (Figure S1).[1−3] The density of fluorescently labeled substrates on each track was then determined by releasing all of the conjugated oligonucleotide using 20 mM DTT and measuring the fluorescence of FAM or TAMRA dyes. Fluorescence was measured using a multimode microplate reader (SpectraMax i3, Molecular Devices), and the density was quantified by using fluorescent-dye-labeled substrates as external standards.

Real-Time Monitoring of the Nanomachine Activity. For a typical reaction, a reaction mixture containing 1 nM DNA walker, 100 pM SNA track, 20 U nicking endonuceases, and 1× NEB CutSmart Buffer was incubated at 37 °C in a 96-well microplate. Fluorescence signals were measured immediately after adding the nicking endonuclease. This measurement was carried out every 1 min using a multimode microplate

https://dx.doi.org/10.1021/acs.analchem.9b04964
Anal. Chem. 2020, 92, 3220−3227

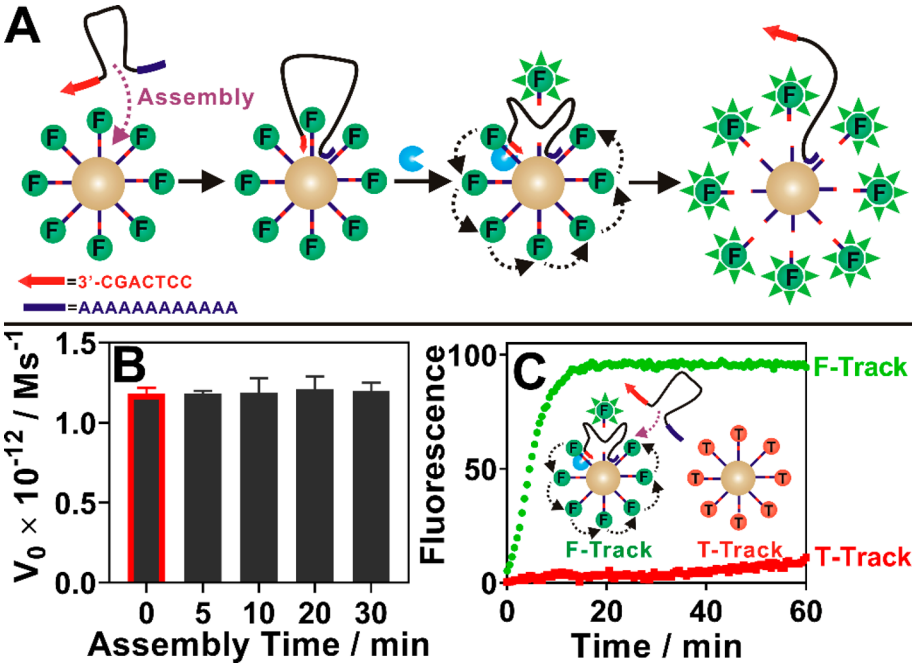

Figure 1. (A) Schematic illustration of the design principle of 3DDNv2.0. A swing-arm DNA walker is designed to contain a nicking recognition domain (red) and a polyA anchor domain (blue). This DNA walker is freely diffused in homogeneous solution and thus can participate in in-solution biorecognition interactions or reactions. Upon addition of the SNA track, this DNA walker will be assembled instantly onto the track via nonspecific adsorption through the polyA anchor. In the presence of the nicking endonuclease, rapid on-particle enzymatic degradation occurs, which cleaves and releases the signal reporters via the nicking cleavage sites. (B) Initial rate of the on-particle biocatalysis as a function of the assembly time of the DNA walker. [Track] = 100 pM, [walker] = 1 nM, [nicking endonuclease] = 20 U. Each error bar represents one standard deviation from triplicate analyses. (C) Kinetic profiles for probing the intraparticle walking of 3DDNv2.0. This is achieved by first priming the DNA walker on a FAM-labeled SNA track and then mixing it with a TAMRA-labeled track and nicking endonuclease (inset). [F-track] = 100 pM, [T-track] = 100 pM, [walker] = 1 nM, [nicking endonuclease] = 20 U.

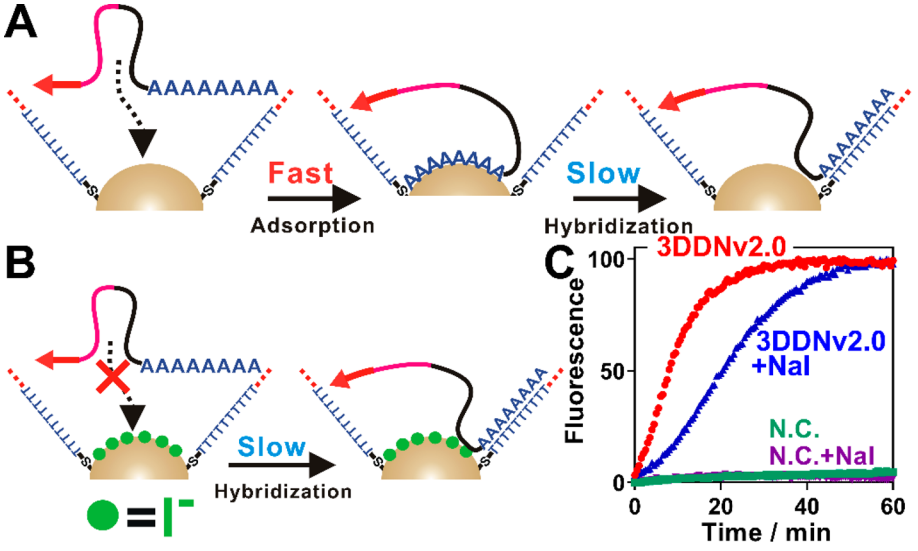

Figure 2. (A) Schematic illustration of a proposed mechanism for assembly of the DNA walker onto an SNA track through the polyA anchor. The proposed assembly process involves a rapid, instant assembly step through nonspecific polyA−AuNP adsorption followed by a slow on-particle diffusion and hybridization with the polyT spacer. (B) Validation of the proposed mechanism by blocking the exposed surfaces of AuNP using iodide ions that prevent the nonspecific adsorption of the polyA anchor. (C) Kinetic profiles of 3DDNv2.0 with an unmodified track (red) and an iodide blocked track (blue). [Track] = 100 pM, [NaI] = 10 μM, [walker] = 1 nM, [nicking endonuclease] = 20 U.

reader to monitor the release of fluorescently labeled substrates. Experimental procedures for nucleic acid and protein analyses as well as for the integration with catalytic DNA circuits and DNA computing are detailed in the Supporting Information.

RESULTS AND DISCUSSION

Design Principle and Mechanistic Study. For concentric amplifiers suffering significant binding hindrance at bionano interface, we proposed to decouple the on-particle biorecognition from the subsequent on-particle biocatalysis. As

https://dx.doi.org/10.1021/acs.analchem.9b04964
Anal. Chem. 2020, 92, 3220−3227

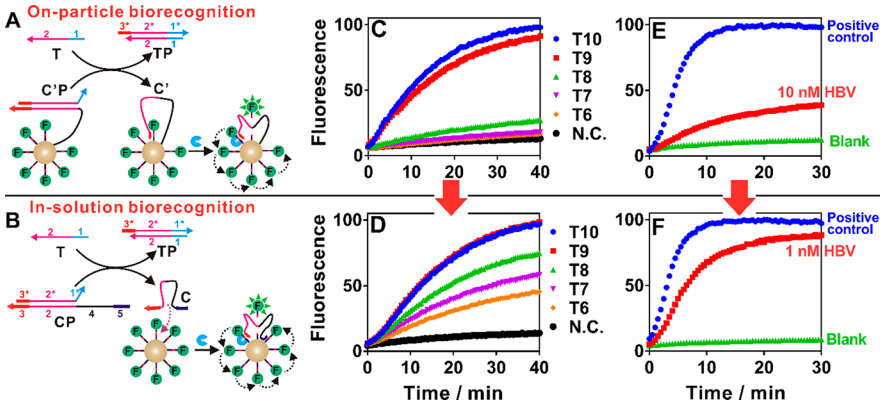

Figure 3. Schematic illustration of (A) on-particle biorecognition vs (B) in-solution biorecognition for activating 3DDN using nucleic acid targets. Kinetic profiles of DNA targets containing varying lengths of toehold domain from 6 nt (T6) to 10 nt (T10) through (C) on-particle strand displacement and (D) in-solution strand displacement. (E) Activation of 3DDN using 10 nM HBV target through on-particle strand displacement. A positive control that contains 100 pM active 3DDNv1.0 was used for fluorescence normalization, where maximum fluorescence generated by the positive control was set to be 100. [3DDNv1.0] = 100 pM, [nicking endonuclease] = 20 U. (F) Activation of 3DDN using 1 nM HBV target through in-solution strand displacement. [Track] = 100 pM, [CP] = 1 nM, [nicking endonuclease] = 20 U.

a case in point, we have recently developed an enzyme-powered 3D DNA nanomachine (3DDNv1.0) where a DNA walker was coconjugated with hundreds of substrates on a single AuNP.[13] When activating this 3DDNv1.0 using a toehold-mediated DNA strand displacement reaction, we found a significant higher energy barrier for the on-particle strand displacement than that in a homogeneous solution.[13] As such, 3DDNv1.0 is an ideal testbed for our aforementioned hypothesis. To do so, we introduced the second generation of 3DDN (3DDNv2.0) that contains a stand-alone swing-arm DNA walker tethered with a polyadenosine (polyA) anchor. This DNA walker can be assembled dynamically onto an SNA track prepared by conjugating hundreds of fluorescently labeled substrates on a 20 nm AuNP (Figure 1A). As the DNA walker contains a nicking recognition site and the substrate contains a complementary nicking cleavage site, rapid on-particle walking and concentric enzymatic cleavage can be achieved in the presence of a nicking endonuclease (Figure 1A).

Although each substrate contains a polythymine (polyT) spacer, the assembly of the DNA walker is not simply a DNA hybridization event. It has been observed that the reaction pathway for hybridization on SNA differed significantly from that in bulk solution, where a single-stranded DNA (ssDNA) first adsorbed onto the AuNP and diffused along the surface until hybridizing with the immobilized DNA.[22] This observation inspired us to design a polyA sequence as an anchor for assembling the DNA walker in 3DDNv2.0. Because of the high affinity between adenosine and the surface of AuNP,[26−28] we anticipate that this polyA anchor would further enhance the initial adsorption of the DNA walker on the track. Indeed, when mixing the walker with the SNA track, we observed a near instant assembly and rapid signal transduction (Figures 1B and S2A). Based on this observation, we further hypothesize that the instant assembly is enabled by the rapid initial adsorption of polyA anchor to the surface of AuNP, followed by the on-particle diffusion and hybridization with the polyT spacer (Figure 2A).

To confirm that the rapid assembly is a result of the initial adsorption, we blocked the exposed surface of the SNA track with iodide ion (I^-). Liu and co-workers have recently demonstrated that I^- was an efficient backfiller for SNA with an affinity stronger than that of adenosine but weaker than that of thiol.[29] As shown in Figure 3B, the treatment of SNA track with I^- significantly reduced the initial rate of the enzymatic reaction, confirming the critical role of adsorption for the rapid assembly of DNA walkers. Despite the slower kinetics, saturated fluorescence signals were achieved for both treated and untreated 3DDNv2.0 systems, suggesting that a stable assembly would still be achieved through polyA−polyT hybridization (Figure 2B). To exclude the possible interference of I^- to enzymatic reactions, we also treated SNA tracks with high concentrations of deoxyadenosine triphosphate (dATP) as another competitive backfiller for the polyA tail. A similar result was also obtained (Figure S3). By understanding the critical role of nonspecific adsorption for assembling the DNA walker, we further propose that an SNA track with low substrate density might perform better kinetically, since it exposes more AuNP surface to mediate nonspecific adsorption. Indeed, compared to a high-density track (~350 substrates per AuNP), the initial rate for the low-density track (~150 substrates per AuNP) was 3 times faster (Figure S4).

The stable assembly enabled by hybridization is also critical to ensure rapid fluorescence signal amplification through the on-particle biocatalysis. Algar et al. have recently shown that the intraparticle movement of biomolecules might involve a "hopping" or "scooting" mechanism, depending on the reversibility of the molecular interaction at the bionano interface.[7] To investigate the exact intraparticle walking mechanism in our system, we primed the DNA walker on a FAM-labeled SNA track (F-track) which was then mixed with a TAMRA-labeled SNA track (T-track) and nicking endonuclease. The observation that fluorescence signals generated predominately from the F-track confirmed that the assembly of the DNA walker was irreversible, which maximized the kinetics of on-particle biocatalysis (Figure 1C). The observation that initial rates of 3DDNv2.0 varied linearly with the concentration of the walker (Figure S1C) but were independent from the track concentrations further confirmed that the walker assembles irreversibly on the SNA track (Figure S5). As such, 3DDNv2.0 that is created through dynamic walker assembly works effectively the same as 3DDNv1.0 created through coconjugation, and there was no compromise in its kinetic performance. More importantly, 3DDNv2.0

https://dx.doi.org/10.1021/acs.analchem.9b04964
Anal. Chem. 2020, 92, 3220−3227

allows for in-solution biorecognition, which is anticipated to be much more efficient and flexible than the on-particle biorecognition.

In-Solution Biorecognition vs On-Particle Biorecognition. We next investigated the effectiveness of in-solution biorecognition by comparing the overall analytical and kinetical performances for analyzing nucleic acids and proteins between 3DDNv2.0 (in-solution biorecognition) and 3DDNv1.0 (on-particle biorecognition). For a fair comparison, the substrate density and number of DNA walkers on each SNA track for both versions of 3DDN were kept the same. All DNA sequences for both versions were also identical, except that the DNA walker (C) in 3DDNv2.0 contains a polyA anchor for the dynamic assembly. To convert a 3DDN into a biosensor, we also introduced a protecting DNA (P) that partially blocked the nicking recognition site on C (domain 3) and thus deactivated the subsequent enzymatic cleavage (Figures 3 and S6). P was designed to contain a toehold domain (domain 1*), so that C could be released from the CP duplex through a toehold-mediated strand displacement in the presence of a target (T). Once C was released, the activity of 3DDN would be restored, which could be detected in real-time by monitoring the fluorescence signal amplification.

We first compared the in-solution biorecognition and on-particle biorecognition for nucleic acid targets (Figure 3). A 10 min preincubation between T and CP was performed either on-particle for 3DDNv1.0 (Figure 3A) or in-solution for 3DDNv2.0 (Figure 3B) to allow sufficient strand displacement. The reaction mixture was then mixed with SNA track (in the case of 3DDNv2.0) and nicking endonuclease to trigger on-particle biocatalysis. When activating 3DDN using DNA targets with toehold lengths varying from 6 nt (T6) to 10 nt (T10), a clear "jump" in restoring nanomachine activity was observed for the on-particle biorecognition from less than 20% for T8 to over 90% for T9, suggesting a significant higher energy barrier exists at the DNA−AuNP interface (Figure 3C). This result was consistent with our previous observation that a much longer toehold (9 nt) was required to trigger a DNA strand displacement reaction on-particle than that in a homogeneous solution.[13] A similar "jump" in signal generation was also observed for strand displacement on SNA by Liang and co-workers who also found that this energy barrier was caused mainly by steric hindrance.[25] When in-solution biorecognition was deployed for 3DDNv2.0, gradual changes in restored activities were observed when altering the toehold from T6 to T10, which was consistent with the theoretical prediction using NuPack (Figure 3D). More importantly, a target with T8 could restore the nanomachine activity by 70% through in-solution biorecognition, whereas only 20% nanomachine activity could be restored through on-particle biorecognition. Despite the use of a longer toehold, the binding hindrance may still attenuate the analytical performance of 3DDN for analyzing targets that are more sensitive to the binding hindrance. As shown in Figure 3C, when designing 3DDNv1.0 for a subgenomic sequence of hepatitis B virus (HBV), only less than 50% activity of the nanomachine could be restored even when a long toehold (10 nt) and high concentration of target (10 nM) were used (Figure 3E). This challenge was effectively addressed by the in-solution biorecognition, where a near 100% activity restoration was observed in the presence of only 1 nM HBV target (Figure 3F).

Having demonstrated that the in-solution biorecognition improves the detection of nucleic acid target, we next investigated the analytical performance of both versions of 3DDN for the detection of proteins. To enable protein detection with minimal changes of the sequence design, we integrated 3DDN with binding-induced formation of a DNA three-way junction (Figure 4), a strategy that we previously

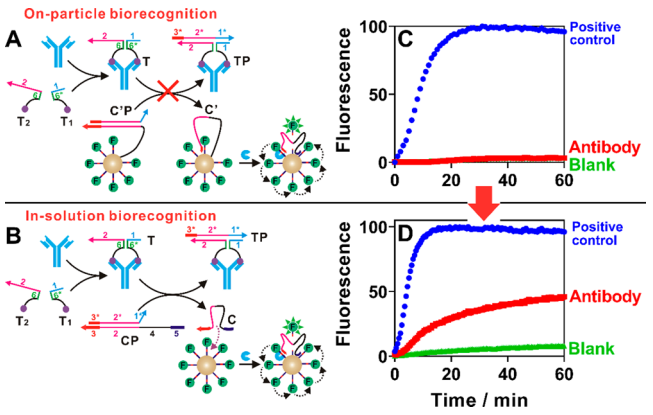

Figure 4. Schematic illustration of (A) on-particle biorecognition vs (B) in-solution biorecognition for activating 3DDN using antibiotin antibodies. (C) Activation of 3DDN using 1 nM antibody through on-particle binding-induced strand displacement. [3DDNv1.0] = 100 pM, [T1] = [T2] = 20 nM, [nicking endonuclease] = 20 U. The on-particle biorecognition was carried out at 37 °C for 30 min. (D) Activation of 3DDN using 1 nM antibody through in-solution binding-induced strand displacement. [Track] = 100 pM, [CP] = 1 nM, [T1] = [T2] = 20 nM, [nicking endonuclease] = 20 U. The in-solution biorecognition was also carried out at 37 °C for 30 min.

invented and has been widely adopted in DNA strand displacement networks for one-step, wash-free protein detection.[30−32] Specifically, we split T into two parts: T_1 and T_2, each of which is extended with a short 6 nt complementary domain (domains 5 and 5*) and then conjugated with an affinity ligand through a flexible linker domain (Figure 4A). The two ligands bind to the same target protein but at different epitopes. Therefore, in the presence of the target protein, T_1 and T_2 will be assembled by the same protein and brought into proximity, leading to the formation of the protein−T_1−T_2 complex. This complex serves effectively as T and triggers the strand displacement with CP either on-particle in the case of 3DDNv1.0 (Figure 4A) or in-solution in the case of 3DDNv2.0 (Figure 4B) and thus activates the amplifier for subsequent fluorescence signal amplification.

As a proof-of-concept, we chose a polyclonal antibiotin antibody (AB) and streptavidin as model target proteins, both of which could be detected by 3DDN using biotin as the affinity ligand (Figures 4 and S7). We expected that the protein−T_1−T_2 complex should be very sensitive to the steric hindrance at the DNA−AuNP interface because of the much larger size than that of the nucleic acid target. Indeed, no fluorescence increase was observed when activating 3DDNv1.0 using 1 nM antibiotin AB, suggesting that the binding complex was unable to activate 3DDNv1.0 through on-particle biorecognition because of the strong steric hindrance (Figure 4C). On the other hand, the same 1 nM antibiotin AB could restore 50% activity of 3DDNv2.0 through the in-solution biorecognition (Figure 4D). We further challenged 3DDNv2.0 using varying concentrations of antibiotin AB and found that as

https://dx.doi.org/10.1021/acs.analchem.9b04964
Anal. Chem. 2020, 92, 3220−3227

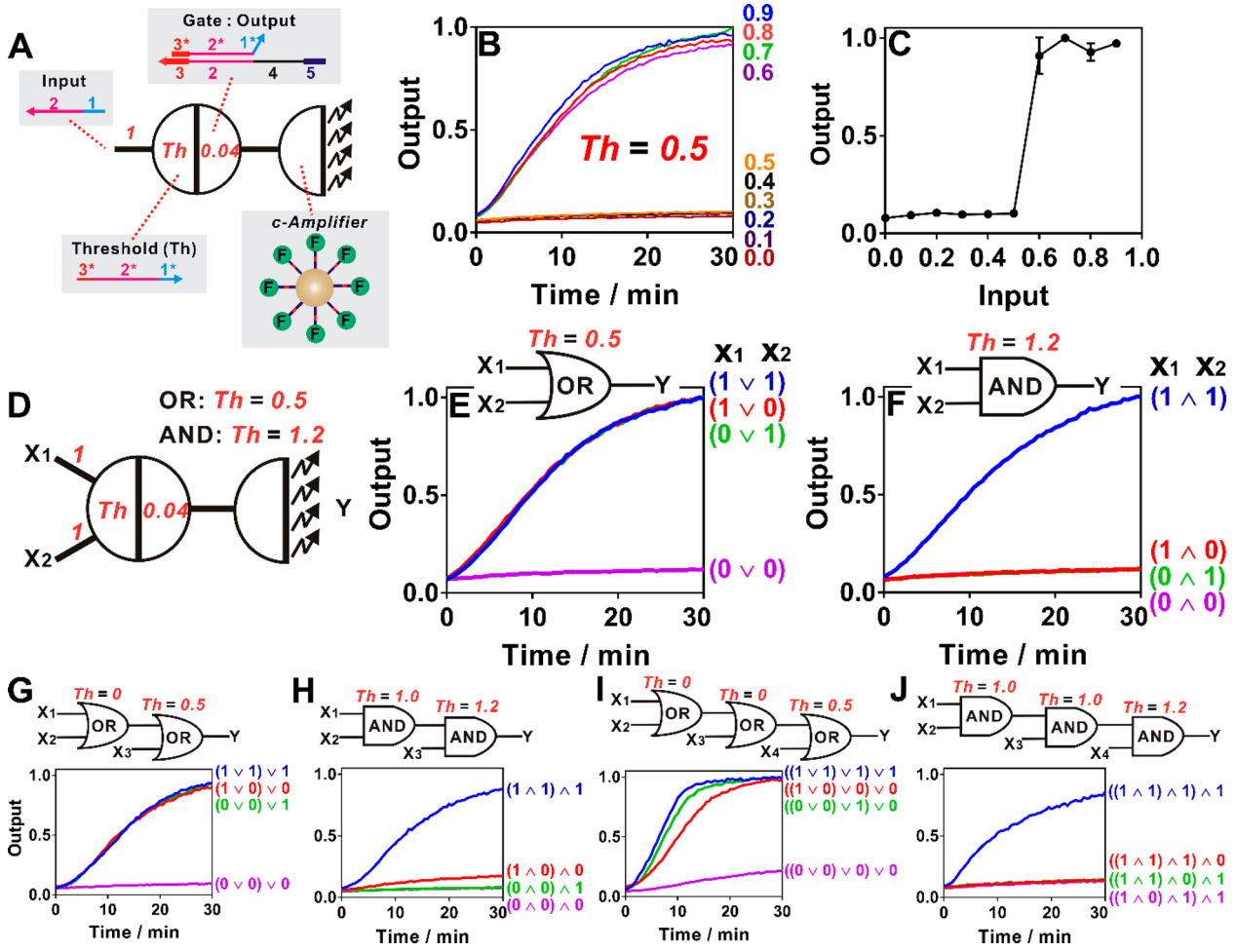

Figure 5. Deployment of 3DDNv2.0 as a plug-and-play amplifier for DNA computing networks. (A) Abstract diagram for a 3DDNv2.0 reporter gate. (B) Kinetics experiments of 3DDNv2.0 reporter gate with threshold. Threshold, gate:output complex, and 3DDNv2.0 reporter were mixed in solution with relative concentrations of 0.5×, 1×, and 0.01×, respectively (1× = 100 nM). Concentration of input strand varied from 0.1× to 0.9×. Fluorescence signals were normalized using an active 3DDNv2.0 as a positive control. (C) Input vs output plot of (B). The output fluorescence at 30 min is plotted against the initial relative concentration of the input. (D) Abstract diagram of a logic circuit that computes either OR or AND, depending on the initial concentration of the threshold. (E) Kinetic profile of a logic OR gate (Th = 0.5×). (F) Kinetic profile of a logic AND gate (Th = 1.2×). Kinetic experiments for multilayered logic gates: OR−OR (G), AND−AND (H), OR−OR−OR (I), and AND−AND−AND (J).

low as 50 pM could be detected by combining the in-solution biorecognition with the on-particle biocatalysis (Figure S7A). A similar observation was also made when streptavidin was used as a model target, where 1 nM streptavidin was able to restore the activity of 3DDNv2.0 by ∼70% through in-solution biorecognition (Figure S7B). As a comparison, less than 20% of the nanomachine activity could be restored through the on-particle strand displacement (Figure S7C). Collectively, our results suggest that the on-particle strand displacement reactions triggered by either nucleic acids or proteins at the DNA−AuNP interface are subject to severe binding hindrance. This challenge can be effectively addressed without compromising any analytical or kinetical performance by streamlining the in-solution biorecognition and on-particle biocatalysis using our strategy.

Adaption of 3DDNv2.0 as a Plug-and-Play Amplifier for DNA Strand Displacement Networks. We finally investigated the adaptability of 3DDNv2.0 as a rapid and plug-and-play concentric amplifier for varying DNA strand displacement networks. As the biorecognition step is decoupled from the on-particle biocatalysis and performed in homogeneous solution, 3DDNv2.0 can be easily plugged into existing DNA strand displacement networks using a translator gate that generates a DNA reporter containing nicking recognition sequence (domain 3) and a polyA anchor (domain 5, Figure 5A). Because the initial input can be completely independent from the final output strand if two translator gates are cascaded, there is no sequence restriction for using the 3DDNv2.0.[33] Upon assembling to the SNA track, the reporter amplifies the detection signal through rapid on-particle biocatalysis. The combination of 3DDNv2.0 with catalytic DNA circuits would allow ultrasensitive detection of biomolecules in an isothermal and wash-free manner. The compatibility with noncovalent DNA catalysis and entropy-driven catalytic DNA circuits was demonstrated in Figures S8 and S9, respectively.

3DDNv2.0 may also serve as a rapid, amplifiable readout for DNA computing. Because a small amount of free input can generate saturated signal output through on-particle biocatalysis, 3DDNv2.0 is expected to be highly tolerant to imperfect inputs and incomplete reactions in cascaded DNA networks. When wired with other DNA circuit motifs, such as a seesaw gate, composable for large-scale DNA computing networks,[34] the self-amplifiable nature of 3DDNv2.0 allows

https://dx.doi.org/10.1021/acs.analchem.9b04964
Anal. Chem. 2020, 92, 3220−3227

rapid signal restoration without the need for additional fuel molecules in one or multiple adjacent layers. As such, the use of 3DDNv2.0 can also reduce the completion time for logic cascades, since the delay time required for circuit computation increased linearly with the number of layers when fuel molecules were used.

Figure 5A illustrates a reporter gate making use of 3DDNv2.0, which is represented by a two-side node similar to that of the seesaw abstraction.[34] The wires represent the input and output DNA strands that are processed by one or more strand displacement or hybridization reactions denoted in the node (strand displacement reactions at each node are detailed in Figure S10). The red number on the wire represents the relative concentration of a free DNA input. The number in the left side of the node represents the relative concentration of a single-stranded threshold strand that depletes input through hybridization. The number in the right side represents a threshold concentration of output that generates saturated fluorescence signal by activating the 3DDNv2.0. Fluorescence kinetic results in Figure 5B confirm that 3DDNv2.0 is fully compatible with DNA circuits, generating ideal ON or OFF values that correspond to the threshold value (0.5). The input-versus-output relationship plotted in Figure 5C reveals a sharp transition at the threshold value, which is more sensitive than previously used molecular reporters.[34]

When one node connects to two or more inputs and a single output, this gate is known as an integrating gate.[34] A two-input integrating gate can compute either OR or AND by setting the threshold at different values (Figure 5D). For an OR gate, the 3DDNv02 will output 1 when the sum of the two inputs is greater than 0.5 and will output 0 otherwise. For an AND gate, the threshold value is set to 1.2. OR and AND computations were demonstrated in Figure 5E,F, respectively. Because as low as a 0.04 input is sufficient to generate saturated fluorescence signal, all computations behaved with near identical rapid kinetic behaviors. Two-layer cascading without additional fuels was also demonstrated with OR−OR (Figure 5G), AND−AND (Figure 5H), and AND−OR (Figure S11). For the OR−OR cascade, the threshold value for the first OR gate is set to be 0, because the final 0.5 threshold is sufficient to block leakages at any layer when all three inputs are 0. Similarly, the threshold of the first AND gate is set to be 1. As shown in the fluorescence kinetic results, the output went to the correct ON or OFF state in all tested cases (Figure 5G,H). Three-layer OR or AND cascades also worked without the need for fuel strands (Figure 5I,J). A slight delay was observed for the three-OR cascade when the input was added in the first layer (Figure 5I). Collectively, our observations suggest that 3DDNv2.0 can be plugged readily into DNA computing networks and help accelerate the computation process. It should also be noted that our strategy is not aimed to replace the seesaw gate but to reduce the uses of fuels whenever possible. For large-scale computing or combined OR−AND layers, fuel molecules are still needed to restore inputs.

CONCLUSION

In conclusion, we have developed a concentric amplifier driven by an enzyme-powered three-dimensional DNA nanomachine (3DDNv2.0), which successfully streamlines in-solution biorecognition and on-particle biocatalysis. Our mechanistic study revealed that a DNA walker with a polyA anchor could be instantly assembled onto an SNA track through adsorption, which was further stabilized through complementary base pairs. This unique property allows for decoupling the biorecognition and biocatalysis elements of a 3DDN without compromising the kinetic performance. More importantly, we demonstrated that the in-solution biorecognition effectively addressed the challenge of binding hindrance faced by the on-particle biorecognition and thus significantly reduced energy barriers for the detection of nucleic acids and proteins. As such, 3DDNv2.0 can be plugged readily into any DNA strand displacement network for rapid signal amplification. We anticipate that 3DDNv2.0 will find wide applications to biosensing and DNA computing. One possible limitation of 3DDNv2.0 is that decoupling 3DDN into a two-component system may hinder its application to intracellular or in vivo sensing. Ongoing efforts toward this challenge include the engineering of 3DDNv1.0 to improve the on-particle biorecognition without splitting essential components. Nevertheless, our success in developing 3DDNv2.0 also demonstrates that it is possible to decouple the biorecognition and signal transduction elements in a homogeneous biosensor without compromising the kinetic performance and thus offers a new solution to design colloidal nanoparticle biosensors and address challenges at bionano interfaces.

ASSOCIATED CONTENT

Supporting Information

The Supporting Information is available free of charge at https://pubs.acs.org/doi/10.1021/acs.analchem.9b04964.

Supporting Experimental Details; supporting Figures S1−S11: absorption spectrum of 3DDNv2.0, kinetics of 3DDNv2.0, mechanistic study of the assembly process, effect of SNA track size, density, and concentration, applications of 3DDNv2.0 to nucleic acid and protein analyses, integration of 3DDNv2.0 with varying catalytic DNA circuits, employment of 3DDNv2.0 as a plug-and-play amplifier for DNA computing; and supporting Table S1: DNA sequences and modifications (PDF)

AUTHOR INFORMATION

Corresponding Authors

Junbo Chen − *Key Laboratory of Green Chemistry & Technology of Ministry of Education, College of Chemistry, Analytical & Testing Centre, Sichuan University, Chengdu 610064, China*; Email: junbochen@scu.edu.cn

Feng Li − *Key Laboratory of Green Chemistry & Technology of Ministry of Education, College of Chemistry, Analytical & Testing Centre, Sichuan University, Chengdu 610064, China; Department of Chemistry, Centre for Biotechnology, Brock University, St. Catharines L2S 3A1, Canada*; orcid.org/0000-0002-2616-5343; Email: fli@brocku.ca

Authors

Peng Yang − *Key Laboratory of Green Chemistry & Technology of Ministry of Education, College of Chemistry, Analytical & Testing Centre, Sichuan University, Chengdu 610064, China; Department of Chemistry, Centre for Biotechnology, Brock University, St. Catharines L2S 3A1, Canada; Department of Chemistry, Waterloo Institute for Nanotechnology, University of Waterloo, Waterloo N2L 3G1, Canada*

Yongya Li − *Department of Chemistry, Centre for Biotechnology, Brock University, St. Catharines L2S 3A1, Canada*

https://dx.doi.org/10.1021/acs.analchem.9b04964
Anal. Chem. 2020, 92, 3220−3227

Sean D. Mason − *Department of Chemistry, Centre for Biotechnology, Brock University, St. Catharines L2S 3A1, Canada*

Fangfang Chen − *Key Laboratory of Green Chemistry & Technology of Ministry of Education, College of Chemistry, Analytical & Testing Centre, Sichuan University, Chengdu 610064, China; Department of Chemistry, Centre for Biotechnology, Brock University, St. Catharines L2S 3A1, Canada;* orcid.org/0000-0002-6589-9198

Rongxing Zhou − *Biliary Surgical Department of West China Hospital, Sichuan University, Chengdu 610064, China*

Juewen Liu − *Department of Chemistry, Waterloo Institute for Nanotechnology, University of Waterloo, Waterloo N2L 3G1, Canada;* orcid.org/0000-0001-5918-9336

Xiandeng Hou − *Key Laboratory of Green Chemistry & Technology of Ministry of Education, College of Chemistry, Analytical & Testing Centre, Sichuan University, Chengdu 610064, China;* orcid.org/0000-0003-2488-2063

Complete contact information is available at: https://pubs.acs.org/10.1021/acs.analchem.9b04964

Notes

The authors declare no competing financial interest.

■ ACKNOWLEDGMENTS

We would like to thank the Analytical & Testing Center of Sichuan University for fluorescence kinetic measurement and we are grateful to Dr. Yanan Tang for her help of experimental design and data analysis. We thank the Fundamental Research Funds for the Central Universities, the Natural Sciences and Engineering Research Council of Canada, the National Natural Science Foundation of China (No. 21705113), the Brock University Advancement Fund, the Science & Technology Support Project of Sichuan Province, the China Scholarship Council (2019YFS0371), and the Brock University Start-Up Fund for financial support.

■ REFERENCES

(1) Zhou, W.; Gao, X.; Liu, D.; Chen, X. *Chem. Rev.* **2015**, *115*, 10575−10636.
(2) Rosi, N. L.; Mirkin, C. A. *Chem. Rev.* **2005**, *105*, 1547−1562.
(3) Howes, P. D.; Chandrawati, R.; Stevens, M. M. *Science* **2014**, *346*, 1247390.
(4) Liu, B.; Liu, J. *Matter* **2019**, *1*, 825−847.
(5) Lei, J.; Ju, H. *Chem. Soc. Rev.* **2012**, *41*, 2122−2134.
(6) Saha, K.; Agasti, S. S.; Kim, C.; Li, X.; Rotello, V. M. *Chem. Rev.* **2012**, *112*, 2739−2779.
(7) Algar, W. R.; Malonoski, A.; Deschamps, J. R.; Blanco-Canosa, J. B.; Susumu, K.; Stewart, M. H.; Johnson, B. J.; Dawson, P. E.; Medintz, I. L. *Nano Lett.* **2012**, *12*, 3793−3802.
(8) Wu, M.; Massey, M.; Petryayeva, E.; Algar, W. R. *J. Phys. Chem. C* **2015**, *119*, 26183−26195.
(9) Algar, W. R.; Jeen, T.; Massey, M.; Peveler, W. J.; Asselin, J. *Langmuir* **2019**, *35*, 7067−7091.
(10) Johnson, B. J.; Algar, W. R.; Malanoski, A. P.; Ancona, M. G.; Medintz, I. L. *Nano Today* **2014**, *9*, 102−131.
(11) Mason, S. D.; Wang, G. A.; Yang, P.; Li, Y.; Li, F. *ACS Nano* **2019**, *13*, 8106−8113.
(12) Mason, S. D.; Tang, Y.; Li, Y.; Xie, X.; Li, F. *TrAC, Trends Anal. Chem.* **2018**, *107*, 212−221.
(13) Yang, X.; Tang, Y.; Mason, S. D.; Chen, J.; Li, F. *ACS Nano* **2016**, *10*, 2324−2330.
(14) Peng, H.; Li, X.-F.; Zhang, H.; Le, X. C. *Nat. Commun.* **2017**, *8*, 14378.
(15) Zhang, H.; Lai, M.; Zuehlke, A.; Peng, H.; Li, X. F.; Le, X. C. *Angew. Chem., Int. Ed.* **2015**, *54*, 14326−14330.
(16) Qu, X.; Zhu, D.; Yao, G.; Su, S.; Chao, J.; Liu, H.; Zuo, X.; Wang, L.; Shi, J.; Wang, L.; Huang, W.; Pei, H.; Fan, C. *Angew. Chem., Int. Ed.* **2017**, *56*, 1855−1858.
(17) Jung, C.; Allen, P. B.; Ellington, A. D. *Nat. Nanotechnol.* **2016**, *11*, 157−163.
(18) Oliviero, G.; Federici, S.; Colombi, P.; Bergese, P. *J. Mol. Recognit.* **2011**, *24*, 182−187.
(19) Xu, J.; Craig, S. L. *J. Am. Chem. Soc.* **2005**, *127*, 13227−13231.
(20) Lytton-Jean, A. K. R.; Mirkin, C. A. *J. Am. Chem. Soc.* **2005**, *127*, 12754−12755.
(21) Randeria, P. S.; Jones, M. R.; Kohlstedt, K. L.; Banga, R. J.; Olvera de la Cruz, M.; Schatz, G. C.; Mirkin, C. A. *J. Am. Chem. Soc.* **2015**, *137*, 3486−3489.
(22) Chen, C.; Wang, W.; Ge, J.; Zhao, X. S. *Nucleic Acids Res.* **2009**, *37*, 3756−3765.
(23) Rodriguez-Quijada, C.; Sánchez-Purrà, M.; de Puig, H.; Hamad-Schifferli, K. *J. Phys. Chem. B* **2018**, *122*, 2827−2840.
(24) Li, Y.; Wang, G. A.; Mason, S. D.; Yang, X.; Yu, Z.; Tang, Y.; Li, F. *Chem. Sci.* **2018**, *9*, 6434−6439.
(25) Yao, D.; Wang, B.; Xiao, S.; Song, T.; Huang, F.; Liang, H. *Langmuir* **2015**, *31*, 7055−7061.
(26) Li, F.; Li, J.; Wang, C.; Zhang, J.; Li, X.-F.; Le, X. C. *Anal. Chem.* **2011**, *83*, 6464−6467.
(27) Zhou, W.; Wang, F.; Ding, J.; Liu, J. *ACS Appl. Mater. Interfaces* **2014**, *6*, 14795−14800.
(28) Pei, H.; Li, F.; Wan, Y.; Wei, M.; Liu, H.; Su, Y.; Chen, N.; Huang, Q.; Fan, C. *J. Am. Chem. Soc.* **2012**, *134*, 11876−11879.
(29) Liu, B.; Wu, P.; Huang, Z.; Ma, L.; Liu, J. *J. Am. Chem. Soc.* **2018**, *140*, 4499−4502.
(30) Li, F.; Lin, Y.; Le, X. C. *Anal. Chem.* **2013**, *85*, 10835−10841.
(31) Tang, Y.; Wang, Z.; Yang, X.; Chen, J.; Liu, L.; Zhao, W.; Le, X. C.; Li, F. *Chem. Sci.* **2015**, *6*, 5729−5733.
(32) Tang, Y.; Lin, Y.; Yang, X.; Wang, Z.; Le, X. C.; Li, F. *Anal. Chem.* **2015**, *87*, 8063−8066.
(33) Seelig, G.; Soloveichik, D.; Zhang, D. Y.; Winfree, E. *Science* **2006**, *314*, 1585−1588.
(34) Qian, L.; Winfree, E. *Science* **2011**, *332*, 1196−1201.